Cloud heights from TOVS Path-B: Evaluation using LITE observations and distributions of highest cloud layers

Claudia J. Stubenrauch, Fadoua Eddounia, Laurent Sauvage

Cloud heights from TOVS Path-B: Evaluation using LITE observations and distributions of highest cloud layers

Claudia J. Stubenrauch and Fadoua Eddounia

Laboratoire de Météorologie Dynamique, Institut Pierre-Simon Laplace, Centre National de la Recherche Scientifique, Ecole Polytechnique, Palaiseau, France

Laurent Sauvage

Leosphere, Inc., Paris, France

Received 20 September 2004; revised 24 April 2005; accepted 7 July 2005; published 6 October 2005.

[1] Cloud height from the TIROS-N Operational Vertical Sounder (TOVS) Path-B climate data set has been evaluated by using vertical profiles of the backscattered radiation at 532 nm from quasi-simultaneous Lidar In-space Technology Experiment (LITE) observations. Two averaging methods for the LITE inversion have been studied. Because of the LITE noise level and the difficulty in determining the vertical structure of thick clouds, we have chosen to apply the inversion on the average backscatter signal of the LITE spots over regions of 1° latitude × 1° longitude, which is also the spatial resolution of the TOVS Path-B data set. The cloud height determined by TOVS corresponds well in general to the height of the ''apparent middle'' of the cloud system with coincidences for 53% of TOVS Path-B low-level clouds within 1 km and for 49% of TOVS Path-B high-level clouds within 1.5 km. In addition, 22.5% of TOVS Path-B low-level clouds are covered by a very thin high cloud layer not detectable by TOVS. Comparing for these cases the TOVS cloud height with the second LITE cloud layer increases the overall agreement for low-level clouds to about 64%. High-level clouds appear more often in multilayer systems (about 75%) and are also vertically more extended. Differences in average cloud height of high-level clouds appear only to be significant (13.3 km from LITE compared to 11.3 km from TOVS Path-B) in the tropics with a large extent of laminar cirrus situated near the tropopause. The height of maximum backscatter of most thick clouds is several hundred meters above ''apparent cloud midlevel,'' whereas thin high-level clouds with underlying lower clouds provide a backscatter signal nearer to apparent cloud midlevel. In the latter case, the retrieved TOVS Path-B cloud height is on average 280 m underestimated. Pressure distributions of the highest cloud layer weighted by effective cloud amount confirmed that high clouds have the lowest pressure in the tropics because of a higher tropopause, and in these regions there are nearly no cloud systems with the highest cloud layer in the middle troposphere. The Southern Hemisphere midlatitudes are mostly covered by low-level clouds. Seasonal differences in the Northern Hemisphere (midlatitudes, with more equally distributed cloud altitudes in winter) are mostly caused by changes over land.

Citation: Stubenrauch, C. J., F. Eddounia, and L. Sauvage (2005), Cloud heights from TOVS Path-B: Evaluation using LITE observations and distributions of highest cloud layers, *J. Geophys. Res.*, *110*, D19203, doi:10.1029/2004JD005447.

1. Introduction

[2] Only satellite observations are capable of giving a continuous survey of cloud properties over the whole globe. Most satellite instruments are radiometers, measuring emitted, reflected and scattered radiation from the Earth's surface, atmosphere and clouds. Cloud physical properties are then determined by inversion models. Several long-term global satellite climatologies of cloud properties exist [e.g., *Rossow and Schiffer*, 1999; *Menzel and Wylie*, 2002; *Stubenrauch et al.*, 2004]; and before using them for climate studies their evaluation is important. This is not always straightforward, because an intercomparison of these global data sets [e.g., *Liao et al.*, 1995; *Jin et al.*, 1996; *Wylie and Wang*, 1997; *Stubenrauch et al.*, 1999b] lacks knowledge of reality, and an evaluation using more sophisticated ground or aircraft measurements [e.g., *Wylie and Menzel*, 1989; *Wang et al.*, 1999] gives often only a point-like insight and not from the same perspective. The whole process of evaluation is certainly an iterative one and needs as many different data sets as possible. Some of these data sets have

0148-0227/05/2004JD005447

already been evaluated using lidar measurements, but these have been undertaken from the ground.

[3] Our approach is a different one by using the first lidar measurements from space by the Lidar In-space Technology Experiment (LITE), providing vertical profiles of backscattered radiation. After describing the inversion algorithms and data sets of TOVS and LITE data in section 2, the collocation of both data sets, including a study of different averaging methods, as well as results on the vertical structure of clouds are presented in section 3. An evaluation of TOVS Path-B cloud height is undertaken in section 4, separately for low-level clouds and high clouds. Section 5 covers zonal distributions of cloud height of the highest layer, weighted by effective cloud amount. These distributions could be useful for the evaluation of general circulation models. Differences between tropics, Northern Hemisphere (NH) midlatitudes and Southern Hemisphere (SH) midlatitudes are stressed, before concluding in section 6.

2. Data Sets and Retrieval of Cloud Properties

2.1. TOVS Path-B

[4] The TIROS-N Operational Vertical Sounder (TOVS) instruments aboard the NOAA Polar Orbiting Environmental Satellites have measured radiation emitted and scattered from different levels of the atmosphere since 1979. The TOVS system consists, in particular, of two sounders: the High resolution Infrared Radiation Sounder (HIRS/2) with 19 IR spectral channels between 3.7 μm and 15 μm and one VIS channel (0.7 μm) and the Microwave Sounding Unit (MSU) with four microwave channels around 5 mm.

[5] The TOVS Path-B data set [*Scott et al.*, 1999] provides global atmospheric temperature and water vapor profiles as well as cloud and surface properties at a spatial resolution of 1° latitude × 1° longitude. At present, the data set covers the time period from July 1987 until June 1995.

[6] The inversion algorithm which converts the measured radiances into physical properties of the atmosphere and surface is based on a fast line-by-line radiative transfer model [*Scott and Chédin*, 1981] and a data set for the initial guess of the atmospheric temperature profile retrieval [*Chevallier et al.*, 1998]. This Thermodynamic Initial Guess Retrieval (TIGR) data set has been generated from a huge collection of radiosonde measurements of temperature, humidity and pressure that are grouped by atmospheric conditions, relating clear sky HIRS radiances to these atmospheric profiles.

[7] Clouds are detected at HIRS spatial resolution (~17 km at nadir) by a succession of threshold tests which have been recently updated [*Stubenrauch et al.*, 2004]. An important part of the cloud detection is the use of simultaneous MSU radiance measurements. Since the latter probe through the clouds, they are used to predict clear sky IR brightness temperatures which are compared to those of the HIRS instrument for all individual pixels to decide if they are cloudy. Other tests, related to spatial heterogeneity, use surface estimates of the atmospheric window channel brightness temperatures at 3.7 μm, 4 μm and 11 μm, in which contributions from water vapor and surface emissivity are removed by a regression from different HIRS brightness temperature channels. Regression coefficients depend on air mass and have been obtained by using least squares fits to the TIGR data set.

[8] To insure more coherence with the MSU spatial resolution (~100 km at nadir), the HIRS radiances are averaged separately over clear pixels and over cloudy pixels within 100 km × 100 km regions. Cloud properties are determined from the averaged cloudy pixel radiances assuming that all cloudy pixels are covered by a single homogeneous cloud layer.

[9] The average cloud top pressure p_{cld} and the average effective cloud emissivity ε_{cld} over cloudy pixels are obtained from four radiances in the 15 μm CO_2 absorption band (with peak responses from 400 to 900 hPa levels in the atmosphere) and one in the 11 μm IR atmospheric window by minimizing a weighted χ^2 [*Stubenrauch et al.*, 1999a]. Empirical weights reflect the effect of the brightness temperature uncertainty within a TIGR air mass class on these radiances at the various cloud levels. The method is based on the coherence of ε_{cld} obtained from the five different wavelengths sensitive to the pressure level of the real cloud:

$$\varepsilon_{cld}(p_k, \lambda_i) = \frac{I_m(\lambda_i) - I_{clr}(\lambda_i)}{I_{cld}(p_k, \lambda_i) - I_{clr}(\lambda_i)} \text{ for } i = 4, 8, \qquad (1)$$

where λ_i is the wavelength of HIRS channel i, p_k is the pressure level k out of 30 levels, I_m is the measured radiance, I_{clr} is the retrieved clear sky radiance and I_{cld} is the calculated radiance emitted by a homogeneous opaque single cloud layer. Effective cloud amount is the product of effective cloud emissivity and cloud fraction.

[10] The accuracy in p_{cld} is limited to the pressure level steps of about 25 hPa to 35 hPa, corresponding to about 250 m to 500 m in the lower troposphere up to 1 km to 1.5 km in the higher troposphere (see section 3.3). The p_{cld} uncertainty can be estimated by the difference in p_{cld} between the solution of the minimized χ^2 and p_{cld} of the second smallest χ^2. Over ocean this uncertainty is about 25 hPa, it is smallest in the Southern Hemisphere (20 hPa) and largest in the Northern hemisphere subtropics (30 hPa). Over land the uncertainty is on average 40 hPa, with a minimum in the tropics (30 hPa) and a maximum in the Northern Hemisphere subtropics (50 hPa).

2.2. LITE

[11] The Lidar In-space Technology Experiment (LITE) [*McCormick et al.*, 1993] provided near-global observations (57°N–57°S) during a 10-day mission of the space shuttle *Discovery* in September 1994. The lidar measured vertical profiles of backscattered radiation at three different wavelengths (355, 532 and 1064 nm). The vertical and horizontal resolutions are 15 m and about 300 m, respectively. Vertical profiles are collected every 740 m. Measurements at 532 nm are the most sensitive to clouds.

[12] An inversion algorithm was developed by the third author on the basis of work by *Young* [1995, 2001] to determine cloud boundaries (cloud top and "apparent cloud base") from these profiles, after averaging them over grids of 1° latitude × 1° longitude (spatial resolution of the TOVS Path-B data set), considering a minimum of 75 individual vertical profiles per grid for a mean lidar profile. Results of this averaging method are compared in section 3 to those using the averages of the retrievals per LITE spot.

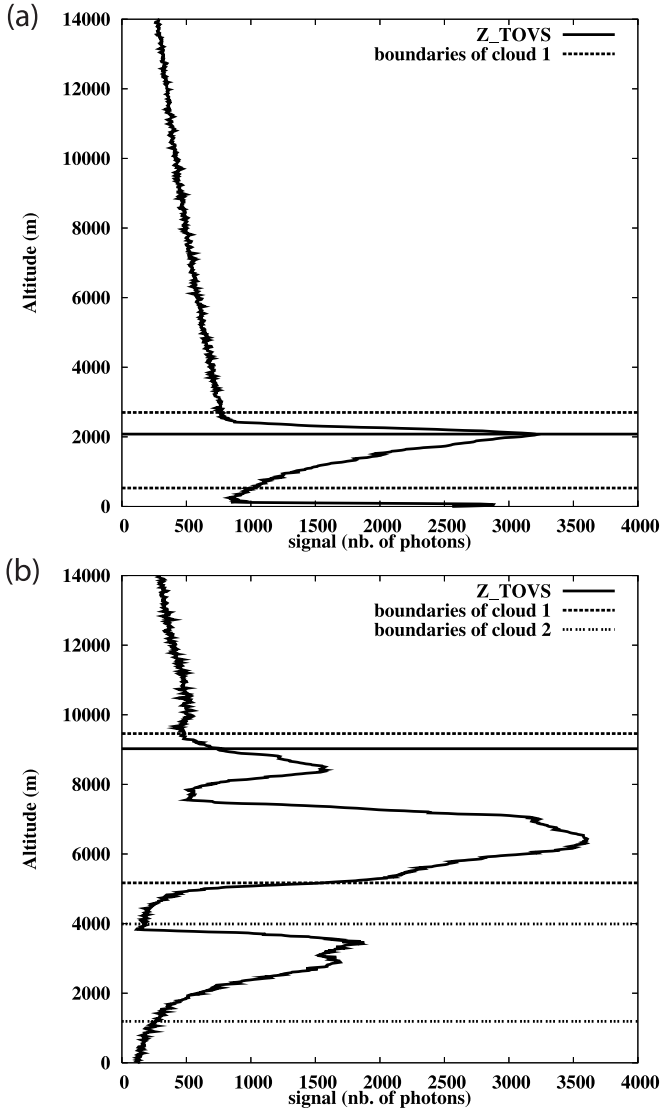

Figure 1. Examples of vertical profiles of the backscatter signal at 532 nm from LITE, averaged over regions of 1° latitude × 1° longitude: (a) case of a low-level single-layer cloud and (b) case of multiple cloud layers. Cloud top and apparent cloud base as obtained from the LITE inversion and TOVS Path-B cloud altitude are also indicated.

Because of the noise of the LITE instrument, results are more reliable when several LITE profiles are averaged [*Young*, 2001]. In the case of clear sky, the backscatter signal increases smoothly with decreasing altitude because of molecular scattering (as can been seen for example in Figure 1 above the low-level cloud). The molecular backscattering profile can be calculated from the atmospheric temperature profile using the hydrostatic equation and the state equation of ideal gases [e.g., *Collis and Russel*, 1976]. In the presence of cloud layers, a strong backscatter peak appears in the signal (see again Figure 1).

[13] Therefore cloud detection along altitude z is based on the variation of the scattering ratio of the measured backscatter signal and the reference molecular backscatter signal, $R(z) = S_{meas}(z)/S_{mol}(z)$, as well as on its derivative $\Delta R(z)/\Delta z$. Even 3 years after the Mt. Pinatubo eruption, clouds were still embedded in a background aerosol layer extending from the surface through the stratosphere. In order to take this effect into account, a reference altitude of $z_{ref} = 18$ km with clear sky above all clouds has been chosen, and a mean ratio $R(z_{ref})$ of all measured LITE profiles has been calculated. Indeed, this ratio is 1.32 instead of the theoretical value of 1. Starting from this altitude downward, a detection threshold R_{cld} is calculated at each altitude level using the running mean of the scattering ratio and its standard deviation over a running interval of 300 m: $R_{cld}(z) = \langle R \rangle + 3\sigma(R\Delta_z)$ and $DR_{cld}(z) = \langle \Delta R/\Delta z \rangle + 2\sigma((\Delta R/\Delta z)\Delta_z)$. The cloud top is detected at $z_{top} = z$ with $R(z) > R_{cld}$ and $-\Delta R/\Delta z > DR_{cld}$. The apparent cloud base is then found at $z_{base} = z$ with $R(z) < R_{cld}$ and $\Delta R/\Delta z < DR_{cld}$. A validated cloud must have a physical thickness of $z_{top} - z_{base} > 100$ m. The apparent cloud base is calculated down to an altitude of 100 m. A variable threshold allows taking into account all cloud layers, especially in the case of multilayering, even when the upper cloud layers lead to a strong attenuation of the signal. In the case of clouds which are uniformly thick over regions of 1° × 1°, the apparent cloud base corresponds to the level to which the lidar penetrates downward (see also section 3.1). The test on the derivative is particularly powerful in the case of large noise as during day. Therefore this method can be applied for night and day measurements, independently of gain variation on the raw signal.

[14] The attenuation of the lidar signal due to the presence of clouds is then calculated by comparing the mean value of the signals, averaged over an interval of 150 m, 100 m above the cloud and 100 m below the cloud, after correction of molecular attenuation. For high subvisible clouds (optical thickness <0.3), an effective optical thickness has been retrieved from the equation: $\tau = -2 \ln(S(z > z_{top})/S(z < z_{base})$. Thresholds both on the signal level above and below the cloud are applied. For very noisy signals (signal-to-noise ratio less than 1) τ has not been computed, and an error code is provided. In addition, a test on the areas chosen above and below the cloud (constant backscattering ratio) as reference values is included to insure the validity of the clear sky assumption. For optical thicker clouds, multiple scattering must be taken into account in the calculation by introducing a coefficient η. For the space-based LITE configuration, η has been found to be about 0.36 [*Platt et al.*, 1999]. In this case, the effective optical thickness will be over three times lower than the true value.

3. Collocation of Data Sets

[15] To make a most direct comparison of cloud height possible, we have first averaged the backscatter profiles of the LITE spots over every 1° × 1° grid containing TOVS observations (from NOAA 11 and NOAA 12 satellites). Figure 2 gives a schematic view of the LITE spots and HIRS spots within a TOVS Path-B 1° × 1° grid. On average, about 90 LITE spots cross a TOVS Path-B grid. In order to have a representative area of LITE spots covering the 1° × 1° grid, we only keep observations with more than 75 LITE spots per TOVS grid.

[16] Reasonable statistics have been obtained by allowing a maximum difference of 3 hours in observation time between TOVS and LITE. Figure 3 presents a geographic

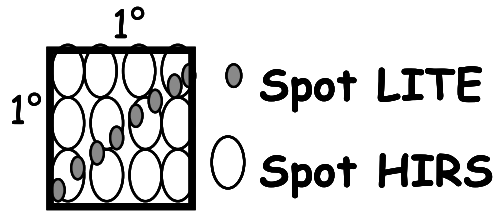

Figure 2. Illustration of coverage of HIRS pixels and the trace of LITE pixels within a 1° latitude × 1° longitude grid.

map with the collocated LITE-TOVS observations. The gray code represents the observation time difference in hours. About 80% (70%) of these collocated data lie within an observation time difference of 2 hours (1 hour). From 9 to 19 September 1994, 1793 quasi-simultaneous TOVS-LITE observations have been collected, of which 1563 observations indicate cloudiness, according to LITE and TOVS Path-B. Because of orbit constellations of the NOAA satellites and the space shuttle, most of the collocated data are in the NH midlatitudes (30°N–60°N) and SH midlatitudes (30°S–60°S), each with about 40%. Only 8% of the statistics are in the tropics (15°N–15°S).

3.1. Averaging Methods for LITE Cloud Height Retrieval

[17] A study of *Young* [2001] has shown that averaging of consecutive LITE profiles is necessary to retrieve useful results, since the signal-to-noise ratio of LITE is much smaller than that of ground-based lidars. However, averaging windows should be chosen over regions with similar profiles. Three cases were considered: thick cirrus, a region with varying cloud vertical structure and a region with constant cloud structure but low signal-to-noise ratio (thin cirrus). In the case of heterogeneity and low signal-to-noise ratio, the optical thickness is underestimated when first averaging and then retrieving instead of averaging the retrieved values. Cloud boundaries are much less affected in these cases.

[18] For a statistically more relevant study, we have applied the LITE retrieval algorithm also to each LITE spot of the collocated data grids at 1° × 1° spatial resolution. The averaged cloud height has then been compared to the cloud height retrieved from the averaged LITE profiles. Figure 4 presents the difference between the altitude of the highest cloud layer retrieved from averaged LITE profiles and averaged upper cloud altitudes retrieved from individual LITE spots as a function of IR heterogeneity σ_{IR} within the grid. The IR heterogeneity is computed as the standard deviation of the IR brightness temperature over the HIRS spots. We distinguish cloud top, height of the maximum backscatter signal and apparent cloud midlevel $z_{mid} = 0.5 * (z_{top} + z_{base})$. At a spatial resolution of 1° × 1°, there are about 90% of all cloud systems for which an apparent cloud base of one of the clouds has been determined. For our analysis we only consider these cases in order to be able to compare also with the apparent cloud midlevel. (Conclusions do not change when using the additional 10% of cases for which the base was set to ground level.) From Figure 4 we deduce that apparent cloud midlevel and height of maximum backscatter from both methods coincide with each other for homogeneous cases ($\sigma_{IR} < 1$ K). With increasing heterogeneity the values obtained from the averaged LITE profiles exceed the mean value of the individual retrievals. The difference is slightly smaller for the apparent cloud midlevel than for the height of maximum backscatter, not exceeding 900 m for $\sigma_{IR} < 10$ K. Cloud top from the averaged LITE profiles is always higher than the mean cloud top of the individual retrievals, increasing from 300 m for $\sigma_{IR} < 1$ K to 2700 m for $\sigma_{IR} > 10$ K. Mean number of cloud layers increases from 0.9 to 1.5. The systematic higher cloud top in the case of first averaging and then retrieving compared to first retrieving and then averaging can be explained by the fact that the retrieval of individual LITE profiles can miss thin cloud layers because of a low signal-to-noise ratio.

[19] The apparent cloud midlevel seems to be the most appropriate to use for a comparison, because it is less

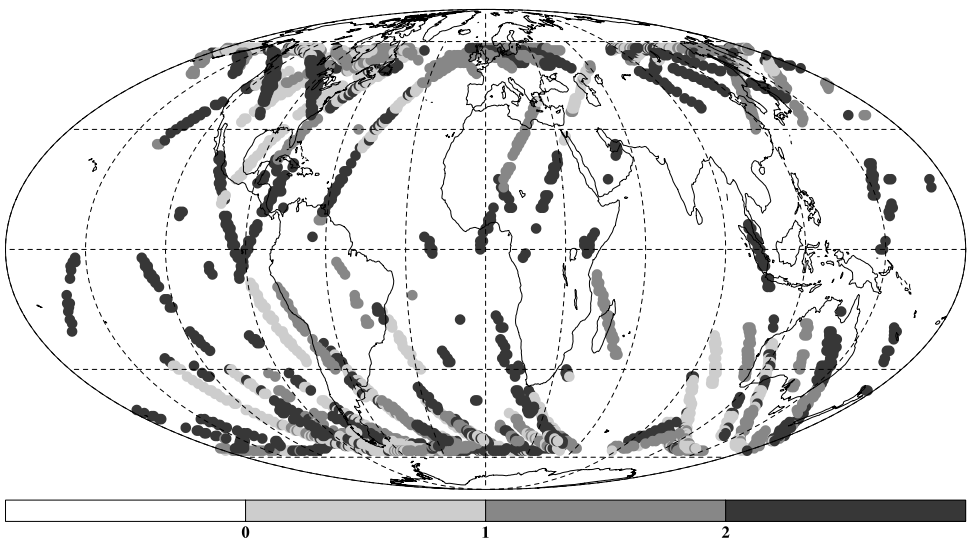

Figure 3. Geographical map of collocated cloudy TOVS-LITE data. The gray scale indicates the difference in observation time in hours.

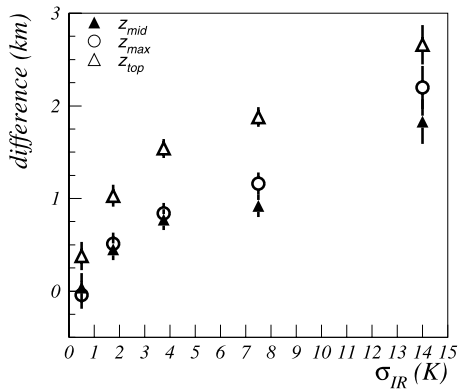

Figure 4. Difference between upper cloud altitude retrieved from averaged LITE profiles and averaged upper cloud altitude retrieved from individual LITE spots within a grid of 1° latitude × 1° longitude as a function of IR heterogeneity within the grid. Cloud altitude is expressed as apparent cloud midlevel, level of maximum backscatter signal, and cloud top level.

sensitive to cloud heterogeneity. However, this level can be biased in the case of optically thick clouds: The base of a thick cloud should be overestimated, because the lidar cannot pass completely through the cloud. Figure 5 presents distributions of the difference between cloud height from the averaged LITE profiles and mean cloud height of the individual LITE retrievals for all clouds, and separately for optically thick and optically thin single-layer clouds. Optically thick single-layer clouds are defined by a ratio of the ground signal to the signal of maximum backscatter of the cloud smaller than 0.1. In general, $z_{\max}$ and z_{mid} differences peak both around 0 km, but for optically thick clouds the peak of the difference is shifted toward −1 km for z_{mid}, whereas the difference is less for $z_{\max}$. This means that z_{mid} determined from every LITE spot within a 1° × 1° region of a thick cloud system is on average about 1 km higher than z_{mid} estimated from the averaged lidar backscatter profile. Probably there are some spots within the 1° × 1° regions which let the lidar more penetrate into the thick layer cloud system.

[20] Considering the evaluation of TOVS cloud height in section 4 which is performed separately for low-level clouds and high clouds, we have investigated differences in z_{mid}, in $z_{\max}$ and in cloud geometrical thickness ($z_{top} - z_{base}$) between both averaging methods for these different cases. Low-level and high clouds are distinguished by p_{cld} ($p_{cld} >$ 680 hPa and $p_{cld} <$ 440 hPa, respectively), according to TOVS Path-B. Table 1 summarizes the results. Differences in z_{mid} vary between −1.14 km for optically thick single low-level clouds and 1.10 km for optically thin single high clouds. The negative differences for single thick clouds can be explained by the fact that the cloud base is overestimated for individual LITE spots for which the clouds are thicker than the average cloud system. In this case, z_{mid} obtained from the averaged LITE profiles would give a better estimate of apparent midlevel of the cloud system. These studies suggest that z_{mid} is only an indication for the midlevel of the cloud field at 1° × 1° spatial resolution, but seems to be the most reasonable variable to indicate the overall height of the cloud field.

[21] It is also interesting to compare cloud geometrical thickness from both averaging methods: from Table 1 we deduce that the thickness of the highest cloud obtained from the averaged LITE profiles is much larger than the difference of average cloud top and average apparent cloud base of the highest layers, especially for high clouds. Compared to an overall cloud geometrical thickness of about 1.6 km (and of about 2.3 km for single-layer clouds) obtained from long-term radiosonde observations [*Wang et al.*, 2000], the first method seems to overestimate cloud geometrical thickness (average of 2.2 km), whereas the second method seems to underestimate it (average of 0.6 km). Nevertheless, both methods agree that high clouds are in general nearly twice as thick as low-level clouds.

[22] The average number of cloud layers as obtained from averaged LITE profiles and the mean number of cloud layers from the individual LITE retrievals within a grid are also displayed in Table 1. In general, the latter is smaller because there are often LITE spots for which no cloud has

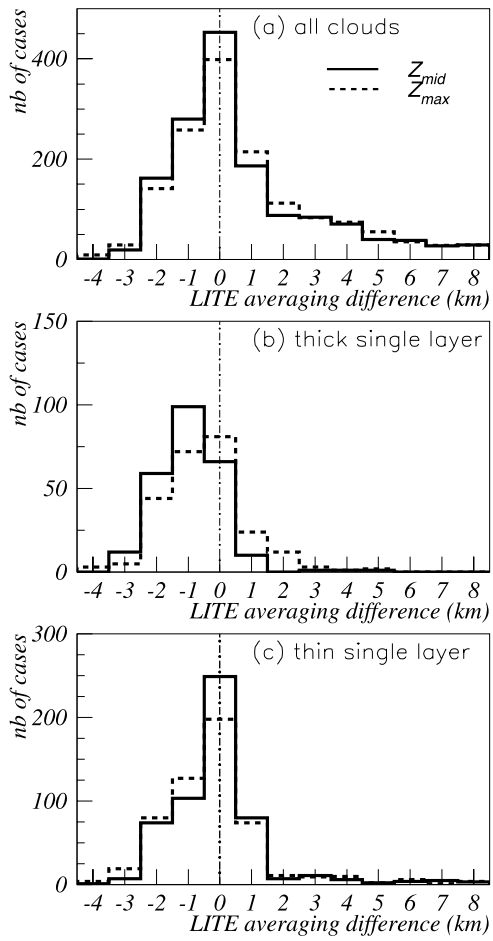

Figure 5. Distributions of difference between upper cloud altitude retrieved from averaged LITE profiles and averaged upper cloud altitude retrieved from individual LITE spots within the grid. Cloud altitude is expressed as apparent cloud midlevel and level of maximum backscatter signal for (a) all clouds, (b) thick single-layer clouds, and (c) thin single-layer clouds. Thick clouds are defined by a ratio of average signal at ground and average signal of maximum backscatter of upper cloud smaller than 0.1.

Table 1. Frequency of Occurrence, Difference in z_{mid} and z_{max} Between the Two Averaging Methods (Retrieval of Averaged LITE Profiles and Average of Retrieved Values Per LITE Spot), Cloud Geometrical Thickness, and Number of Cloud Layers From Both Averaging Methods for Different Cloudy Scenes[a]

	Occurrence, %	z_{mid} Difference, km	z_{max} Difference, km	$z_{top}-z_{base}$, km	$\langle z_{top}\rangle-\langle z_{base}\rangle$, km	Number of $z_{top}-z_{base}$	Number of $\langle z_{top}\rangle-\langle z_{base}\rangle$
All clouds	100	0.73	0.84	2.22	0.60	2.1	1.3
			Low Clouds				
All low	51	0.36	0.31	1.65	0.44	1.9	1.1
Single low	36	−0.44	−0.55	1.75	0.47	1.0	1.0
Single low thick	8	−1.14	−0.95	1.66	0.71	1.0	1.4
Single low thin	28	−0.33	−0.43	1.77	0.40	1.0	0.8
			High Clouds				
All high	32	1.51	1.83	2.87	0.85	2.5	1.5
Single high	10	0.19	0.72	3.67	1.15	1.0	1.2
Single high thick	5	−0.67	0.28	4.55	1.97	1.0	1.5
Single high thin	5	1.10	1.21	2.82	0.37	1.0	0.9

[a]Low-level and high clouds are distinguished according to TOVS Path-B. Thick and thin clouds are distinguished according to the ratio between ground signal and signal of maximum backscatter of cloud.

been detected (in about 70% of all thin single-layer and about 10% of all thick single-layer cloud systems). For single-layer low-level clouds the mean cloud layer number within the grid is also about one, whereas for single-layer high clouds the mean cloud layer number is slightly higher. For single-layer thick clouds (15% of all clouds), as obtained from the averaged LITE profiles, the mean number of cloud layers from individual LITE spots is about 1.5.

3.2. Cloud Vertical Structure of the Data Set

[23] According to TOVS Path-B, the data set contains 51% low-level clouds of which 70% are single layered and 32% high clouds of which 33% are single layered. The pressures of 680 hPa and 440 hPa correspond approximately to altitudes of 3 km and 7 km, respectively.

[24] According to the LITE inversion, 55% of the $1° \times 1°$ grids are covered by single-layer clouds and 45% by multilayer cloud systems. These results are in close agreement to 58% single-layer clouds from long-term radiosonde observations [*Wang et al.*, 2000]. Whereas 62% of the maritime clouds appear as single layers, continental cloud systems are more often multilayered (55%). Distinguishing low-level clouds and high-level clouds by their cloud top altitude (3 km and 7 km, respectively) according to LITE, the data set contains 34% low-level clouds of which most (94%) are single layered and 46% high clouds of which most (76%) appear with lower clouds underneath. These results are summarized in Tables 2 and 3.

[25] Comparing these results to those obtained by TOVS Path-B leads already to the assumption that LITE observations are more sensitive to high thin clouds. The latter could be misidentified by TOVS as low-level clouds in the case of multilayer cloud systems. We will investigate this in the following in more detail.

Table 2. Frequency of Occurrence of Single-Layer and Multilayer Clouds According to LITE Inversion

	Single-Layer Clouds, %	Multilayer Clouds, %
All	55	45
Ocean	62	38
Land	45	55

3.3. Conversion of Cloud Pressure to Cloud Height

[26] Since the LITE cloud altitude is given in km, we convert the TOVS cloud pressure by using profiles from the National Meteorology Center (NMC) which provide altitudes corresponding to standard pressure levels (1000, 850, 700, 500, 400, 300, 250, 200, 150 and 100 hPa) for each of the LITE measurements. These profiles are obtained from the nearest forecast, and they depend on the meteorological situation. Like the other LITE data, they have been averaged over each TOVS grid. On average, 800 hPa correspond to ~2 km, 700 hPa to ~3 km, 400 hPa to ~7 km, 300 hPa to ~9 km, 200 hPa to ~12 km and 100 hPa to ~16 km. Differences between tropical and midlatitude profiles are larger in the upper part of the troposphere (up to 1 km for pressures lower than 400 hPa), with a higher altitude for the same pressure in the tropics.

[27] To estimate an uncertainty introduced by this height conversion, we compared these profiles with those determined from TOVS Path-B virtual temperature—pressure profiles, averaged over the month of September 1994. Differences are slightly larger in the upper troposphere ($p <$ 440 hPa), with about 140 m in the midlatitudes and 90 m in the tropics, than in the lower troposphere ($p >$ 680 hPa), with about 100 m in the midlatitudes and 45 m in the tropics.

4. Evaluation of Cloud Height

[28] Figure 1 presents two examples of backscatter profiles averaged over the $1° \times 1°$ grids. Cloud top and apparent base within the cloud system from the LITE inversion as well as the retrieved TOVS Path-B cloud pressure are added. In the first example, a situation with

Table 3. Frequency of Occurrence of Low-Level Clouds and High Clouds According to TOVS Path-B and to LITE

	TOVS Path-B		LITE	
	Low Clouds, %	High Clouds, %	Low Clouds, %	High Clouds, %
All	51	32	34	46
Single Layer	70	33	94	24
Multilayer	30	67	6	76

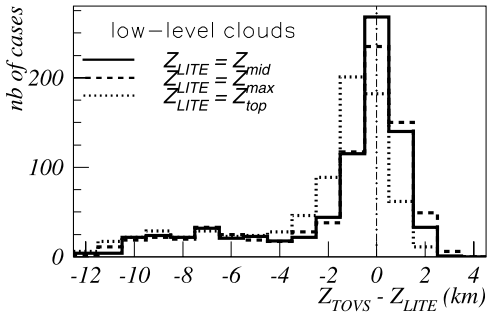

Figure 6. Distributions of difference between TOVS Path-B cloud altitude and altitude of the highest cloud layer detected by LITE for TOVS Path-B low-level clouds. LITE altitude is expressed as apparent cloud midlevel (solid line), level of maximum backscatter signal (dashed line), and cloud top level (dotted line).

low-level clouds, the TOVS Path-B cloud height corresponds within a few meters to the maximum backscatter signal of the cloud. We also observe that the maximum backscatter signal of the low-level cloud system lies slightly above the apparent midlevel of the cloud system. The second example represents a cloud system with several vertical cloud layers, and in this case the TOVS Path-B cloud height lies well within the limits of the highest cloud. Even if there are three maxima of backscattering to be seen in Figure 1, the LITE inversion has distinguished only two cloud layers, because the difference between apparent cloud base of the highest cloud and cloud top of the next cloud layer is less than 300 m. Since the LITE spots have been averaged over a region of $1° \times 1°$, it is difficult to tell if there were really two distinguished cloud layers over this region or if this is one cloud layer breaking up at different places within the $1° \times 1°$ regions.

[29] In the following statistical analysis, we evaluate the TOVS Path-B cloud height separately for low-level clouds and high clouds ($p_{cld} > 680$ hPa and $p_{cld} < 440$ hPa, respectively).

4.1. TOVS Path-B Low-Level Clouds

[30] Figure 6 represents distributions of differences between TOVS Path-B cloud height and LITE cloud height for situations with TOVS Path-B low-level clouds. The LITE cloud height is expressed as apparent cloud midlevel (see definition in section 3.1, full line), as height of the maximum backscatter signal (broken line) and as height of the cloud top (see sections 2.2 and 3.1 and broken lines in Figure 1). The latter height seems to be mostly 1 km higher than the TOVS Path-B cloud height, whereas the comparison with the other two height definitions leads to a peak around 0 km, with 53% and 49% of the clouds within 1 km difference, respectively. Considering the time difference between the observations (on average 90 min) and the different spatial coverage of both instruments (the LITE spots cover on average only 1% of the TOVS Path-B grid), this agreement is very good. For situations with the same cloud identification (difference <2 km), the mean difference between TOVS Path-B cloud height and LITE apparent cloud midlevel is 43 m.

[31] We also observe 30% of situations in which the LITE cloud height is considerably larger (>3 km) than the one from TOVS Path-B. These could be cases with very thin high clouds (to which TOVS is not sensitive) with underlying low-level clouds. To investigate this assumption further, we consider cloud height differences between TOVS and LITE (only apparent midlevel) separately for situations in which LITE has detected a single cloud layer, presented in Figure 7a, and multiple cloud layers (full line in Figure 7b). Indeed, large differences between TOVS and LITE cloud heights occur in the case of multiple cloud layers (on average 6.2 km), whereas 70% of all single-layer TOVS low-level clouds agree within 1 km with the LITE apparent cloud midlevel. The agreement for single-layer low-level clouds decreases slightly to 66% in the case of thick clouds (ratio between ground signal and signal of maximum backscatter of the cloud <0.1), which are only 22% of all single-layered low-level clouds, according to Table 1.

[32] An analysis of the optical thickness retrieved by LITE has shown that about 75% of cases with multiple cloud layers consist of a highest cloud layer with $\tau < 0.1$, within the noise level of TOVS [*Wylie et al.*, 1995]. By comparing for these cases the TOVS Path-B cloud height with the apparent cloud midlevel of the second LITE cloud layer, the difference peaks again around 0 km, as presented by the broken lined distribution in Figure 7b. For these cases, 65% of the TOVS Path-B cloud heights lie within 1 km difference of the second cloud layer of the LITE inversion. By taking this effect into account, the overall agreement within 1 km between TOVS Path-B cloud height

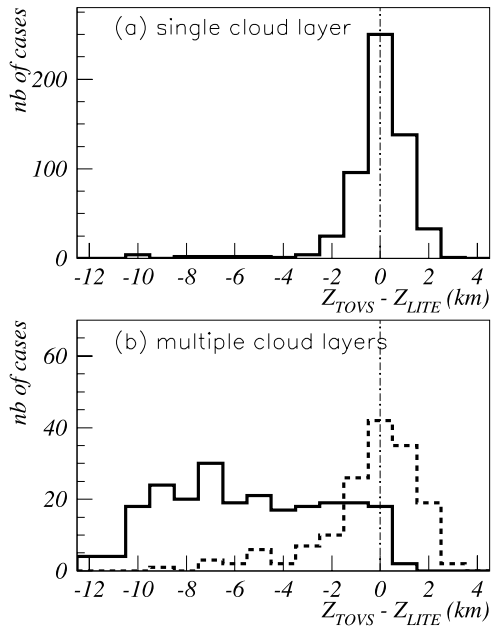

Figure 7. Distributions of difference between TOVS Path-B cloud altitude and altitude of the highest cloud layer detected by LITE for TOVS Path-B low-level clouds. LITE altitude is expressed as apparent cloud midlevel. (a) LITE single-layer clouds. (b) LITE multiple-layer clouds: difference between TOVS Path-B cloud altitude and LITE midlevel of highest cloud (solid line) and second-highest cloud (dashed line) if τ of highest cloud <0.1.

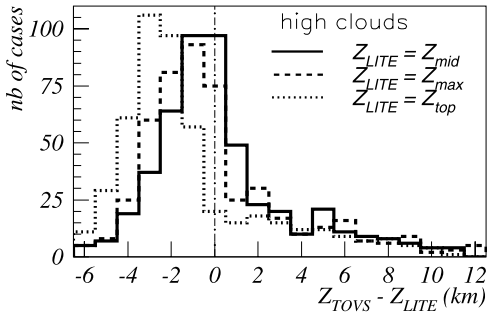

Figure 8. Distributions of difference between TOVS Path-B cloud altitude and altitude of the highest cloud layer detected by LITE for TOVS Path-B high-level clouds. LITE altitude is expressed as apparent cloud midlevel (solid line), level of maximum backscatter signal (dashed line), and cloud top level (dotted line).

and LITE apparent cloud midlevel for TOVS Path-B low-level clouds would be 64%.

4.2. TOVS Path-B High-Level Clouds

[33] For situations in which TOVS Path-B identified high clouds, Figure 8 shows differences between TOVS Path-B cloud height and LITE cloud height, again for the same three cloud height definitions as in section 4.1. First, the differences between LITE cloud top, height of maximum backscatter and cloud midlevel are larger than for low clouds. This can be explained by a larger vertical extent of the high-level clouds (see Table 1). The peak of the difference between TOVS Path-B cloud height and LITE apparent cloud midlevel is again centered around 0 km, whereas compared to the height of maximum backscatter the peak is slightly shifted toward −1 km and compared to cloud top even −3 km. The distributions are slightly broader than for low-level clouds. This can be again explained by a larger vertical extent as well as larger spatial heterogeneity of these clouds.

[34] 49% of all TOVS high-level clouds have a height determined within 1.5 km of the LITE cloud midlevel. 14% of TOVS high-level clouds have been identified as lower-level clouds by LITE ($z_{TOVS} - z_{mid} > 4$ km). Most of these cases include only one cloud layer over the LITE path (Figure 9a). For these situations, the TOVS Path-B cloud cover is slightly smaller (84% compared to 95%) and the IR brightness temperature heterogeneity is slightly larger (9 K compared to 8 K). So, most probably these situations are low-level cloud fields with some high-level clouds which have not been traced by the LITE path in the TOVS Path-B grid. The difference distribution of multiple-layer clouds (Figure 9b) in the case of TOVS Path-B high clouds is not as dramatically shifted toward negative values as the one for TOVS Path-B low-level clouds, because the minimum cloud height of TOVS Path-B corresponds to about 6.5 km. Figure 9b also presents a difference distribution for cases with the height of the maximum backscatter signal close to the apparent midlevel of the cloud system (within 150 m) instead of more above apparent midlevel which is the case for most single-layer high clouds (on average about 530 m).

[35] By comparing single cloud layer and multiple cloud layer situations for which both cloud identifications agree (difference smaller than 1.5 km), the mean values of TOVS cloud height and LITE cloud midlevel are about −40 m and −280 m, respectively. This means that in the case of multiple-layer clouds, the TOVS Path-B cloud height is about 280 m below the apparent midlevel of the most upper cloud. This is a slightly smaller discrepancy than the one foreseen by the CO_2 slicing technique in studies of *Menzel et al.* [1992] and *Baum and Wielicki* [1994].

[36] As mentioned above, the structure of the vertical backscatter profiles of single-layer high clouds and of high clouds with underlying lower clouds is different: By analyzing the difference between height of maximum backscatter and apparent cloud midlevel separately, one finds that on average the height of maximum backscatter at 523 nm is about 524 m above the apparent cloud midlevel for single-layer high clouds, whereas in the second case both heights are much closer (166 m above). In the second situation, the IR radiation should go deeper into the cloud which would explain the larger difference between TOVS Path-B cloud height and LITE apparent cloud midlevel. The difference in $z_{\max} - z_{mid}$ can also be explained by the fact that the lidar does not penetrate as much a thick cloud as a thin cloud. For single-layer thick high clouds $z_{\max} - z_{mid}$ is about 780 m, whereas the difference is only 280 m for single-layer thin high clouds. The distinction between thick and thin clouds is the same as in section 3.1.

5. Zonal Distributions of Cloud Altitude

[37] Figure 10 provides distributions of cloud height from TOVS Path-B (full line) compared to the apparent cloud

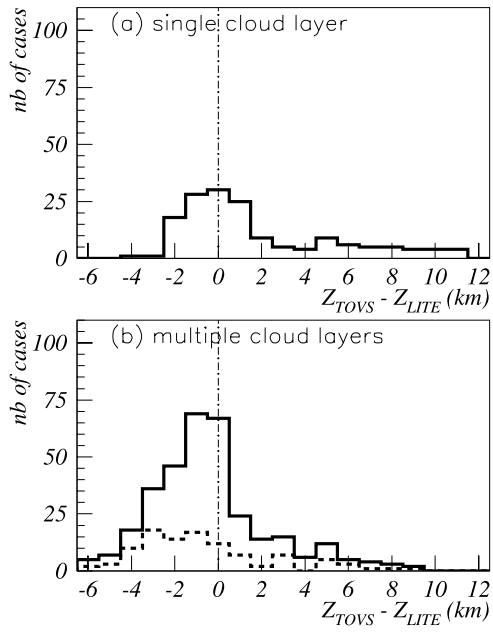

Figure 9. Distributions of difference between TOVS Path-B cloud altitude and altitude of the highest cloud layer detected by LITE for TOVS Path-B high-level clouds. LITE altitude is expressed as apparent cloud midlevel. (a) LITE single-layer clouds. (b) LITE multiple-layer clouds: difference between TOVS Path-B cloud altitude and LITE midlevel of highest cloud for all cases (solid line) and difference for cases with $z_{\max}$ close to z_{mid}.

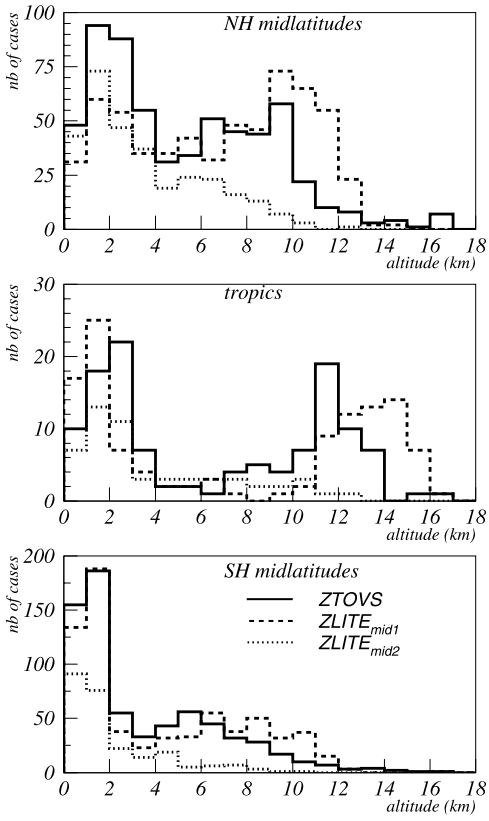

Figure 10. Distributions of cloud altitude as determined by TOVS Path-B (solid line), apparent midlevel of LITE highest cloud layer (dashed line), and apparent midlevel of LITE second-highest cloud layer (dotted line) for NH midlatitudes, tropics, and SH midlatitudes.

midlevel of the highest cloud layer (broken line) and the second-highest cloud layer (dotted line, in the case of multilayer clouds) from LITE, separately for NH midlatitudes, tropics and SH midlatitudes. These distributions first show that clouds extend highest in the tropics, which is expected because of the higher altitude of the tropopause: Average high-level ($z > 7$ km) cloud heights from LITE (TOVS Path-B) are 13.3 km (11.3 km) in the tropics, 9.9 km (9.6 km) in NH midlatitudes and 9.3 km (9.3 km) in SH midlatitudes. The smallest extend of cloud heights occurs in the SH midlatitudes, probably due to the lack of land. The shapes of the cloud height distributions look different in the three latitude bands: Whereas there are nearly no midlevel clouds in the tropics, leaving two distinct distributions of highest cloud height with peaks around 1.5 km and 14.5 km from LITE (or 2 km and 12 km from TOVS), the NH midlatitudes show cloud heights at all levels with only slight maxima around 1.5 km and 10.5 km from LITE (1.5 km and 9.5 km from TOVS). The SH midlatitudes are mostly covered by low-level clouds. This distribution has mostly one strong peak around 1.5 km. The larger contribution of higher cloud altitudes from LITE has already been explained in section 4 by the higher sensitivity of LITE to very thin cirrus and by a slight underestimation of TOVS cloud height of thin cirrus. A significant difference of 2 km (or about 50 hPa) in average cloud height of high-level clouds, however, only appear in the tropics, because these regions have a large extent of laminar cirrus near the tropopause, about 14% as has been shown by *Winker and Trepte* [1998].

[38] Figure 10 also provides distributions of the second highest apparent cloud midlevel from LITE in the case of multiple cloud layers. Information of these clouds cannot be given by TOVS or any other passive remote sensing instrument: for 61% in the NH midlatitudes, for 49% in the tropics and for 37% in the SH midlatitudes. These distributions are quite broad, but peak around 1.5 km in the first two latitude bands and at 0.5 km in the SH midlatitudes.

[39] Since TOVS Path-B provides cloud data of 8 years, we present in the following statistically more significant altitude distributions of the highest cloud layer in these three latitude bands as well as their seasonal variation. Cloud pressure is a measure of the atmospheric mass from the cloud level to the top of the atmosphere, and hence for radiation it is a more natural vertical coordinate than geometrical height. Figure 11a presents frequency distributions of TOVS pressure of the highest cloud layer, weighted by effective cloud amount and normalized to total cloud amount, corresponding to the same statistics as in Figure 10 (10 days in September 1994) and the same latitude bands. To test the representativeness of these statistics we have reported in Figure 11b the same distributions averaged over fall (September to November) from 1987 to 1994. Compared to the collocated statistics in September 1994, the distributions look similar, with only slightly lower altitudes of high-level clouds and low-level clouds in the tropics.

[40] Figure 12a presents annual distributions of pressure of the highest cloud layer weighted by effective cloud amount, separately for the tropics (full line), NH midlati-

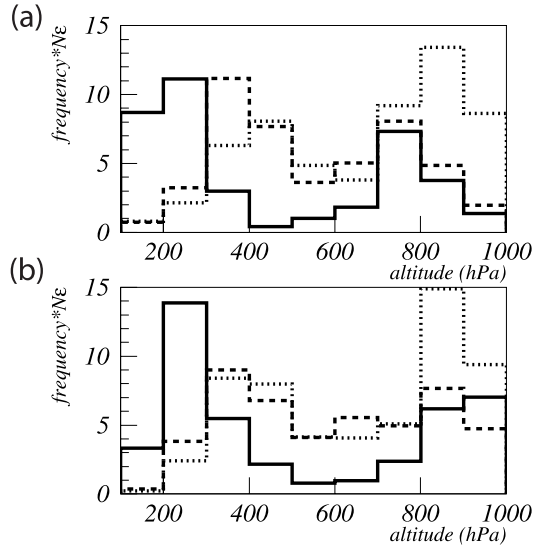

Figure 11. Effective cloud amount weighted frequency distribution of TOVS Path-B pressure of highest cloud layers in the tropics (solid line), NH midlatitudes (dashed line), and SH midlatitudes (dotted line) using (a) statistics of 10 days in September 1994 of collocated TOVS-LITE data set and (b) 8-year averages over fall (September, October, and November) from 1987 to 1994.

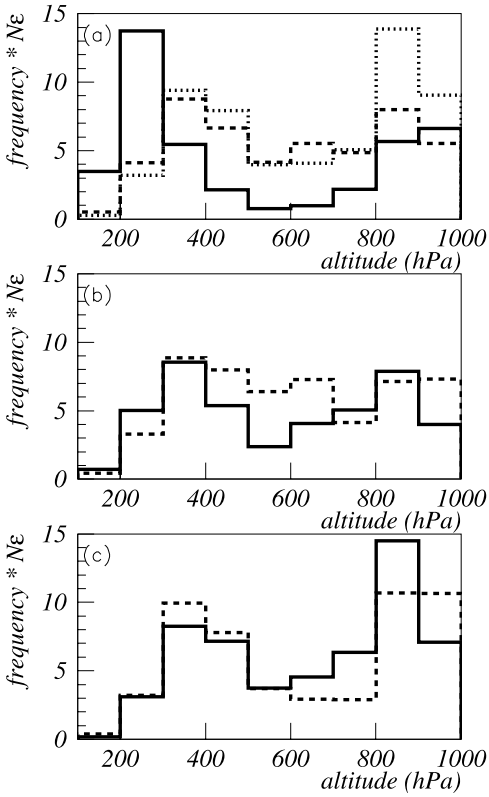

Figure 12. (a) Annual effective cloud amount weighted frequency distribution of TOVS Path-B pressure of highest cloud layers in the tropics (solid line), NH midlatitudes (dashed line), and SH midlatitudes (dotted line). (b) Effective cloud amount weighted frequency distribution of TOVS Path-B pressure of highest cloud layers in NH midlatitudes during summer (solid line) and winter (dashed line). (c) Effective cloud amount weighted frequency distribution of TOVS Path-B pressure of highest cloud layers in SH midlatitudes during summer (solid line) and winter (dashed line). All distributions are 8-year averages.

tudes (broken line) and SH midlatitudes (dotted line). In the tropics, the cloud altitude distribution does not change much during the seasons (not shown), with an effective uppermost high-cloud amount of about 23% and effective uppermost low-level cloud amount of 15%. The effective uppermost midlevel cloud amount is only 4%. Comparing NH and SH midlatitudes, the effective amounts of uppermost high-level and midlevel clouds are about the same (12% and 16%, respectively), whereas effective uppermost low-level cloud amount is much higher in the SH midlatitudes (28% compared to 19%). Figures 12b and 12c present altitude distributions of the highest cloud layers during summer (June to August in NH and December to February in SH, full line) and winter (December to February in NH and June to August in SH, broken line) in the NH midlatitudes and in the SH midlatitudes, respectively. Whereas the seasonal variation in the SH midlatitudes is small, it is interesting to note that in the NH midlatitudes during winter cloud altitudes seem to be more equally distributed within the atmosphere compared to a summer distribution with two distinctive peaks around 350 hPa and 850 hPa. These distributions can be quite useful for the evaluation of climate models. For such a comparison as well as for comparisons with the following figures, only the highest cloud layers of the climate model simulations, as observed from space, have to be considered [*Stubenrauch et al.*, 1997].

[41] For a more detailed investigation of the distribution of the highest cloud layers in these three latitude bands, we consider two-dimensional frequency distributions of effective cloud amount and pressure of the highest cloud layer. Frequencies of occurrence are divided over ten effective cloud amount intervals and seven different cloud pressure intervals. The sum over these 70 two-dimensional intervals is scaled to 100%. Figure 13a presents such a distribution for the tropics. As in Figures 10–12, Figure 13a makes it clear again that in the tropics highest cloud layers appear in the upper troposphere or in the lower troposphere, not in the middle troposphere. Since the TOVS data only give information on the highest cloud layer of multilayer cloud systems, the middle troposphere can still be cloudy underneath systems with high clouds. It is interesting to note, however, that a regional study using ground-based radar data [*Mace and Benson-Troth*, 2002] has also revealed mostly cirrus and boundary layer clouds in the tropics. Uppermost high-level clouds appear with all effective cloud amounts, having two slight maxima of relatively transparent and opaque clouds around 180 hPa. By separating land and ocean, one observes that there are more opaque high-level clouds, linked to convection, over land than over ocean. Whereas uppermost low-level clouds appear mostly as cumulus (small effective cloud amount) over land, their distribution in effective cloud amount is more smeared out, and there are also many low stratus clouds (large effective cloud amount) over ocean.

[42] Figures 14a and 14b present the two-dimensional distributions averaged over NH midlatitudes and SH midlatitudes. As in Figures 10–12, Figures 14a and 14b reflect that high-level clouds are situated lower than in the tropics. One also observes that there are more uppermost thin high-level clouds and more midlevel clouds in the NH than in the SH. The SH midlatitudes are mostly covered by uppermost low-level clouds at all effective cloud amounts, but with slight maxima at both ends of effective cloud amount. To investigate differences in seasonal variations between NH and SH midlatitudes, we consider the two-dimensional distributions of effective cloud amount and pressure of the highest cloud layer, separately above ocean in Figures 15a–15d and above land in Figures 16a–16d. The ocean distributions in Figure 15 for NH and SH midlatitudes are quite similar, with slightly larger cloud pressures for high-level and for low-level clouds in the SH midlatitudes. The land distributions in Figure 16 for both hemispheres also look quite similar, with much more uppermost thin cirrus over land in summer than in winter. The more equally distributed cloud layers within the NH midlatitude atmosphere in Figure 12b can be mostly explained by seasonal changes over land.

6. Conclusions

[43] Cloud height from the TOVS Path-B climate data set has been evaluated by using vertical profiles of the back-

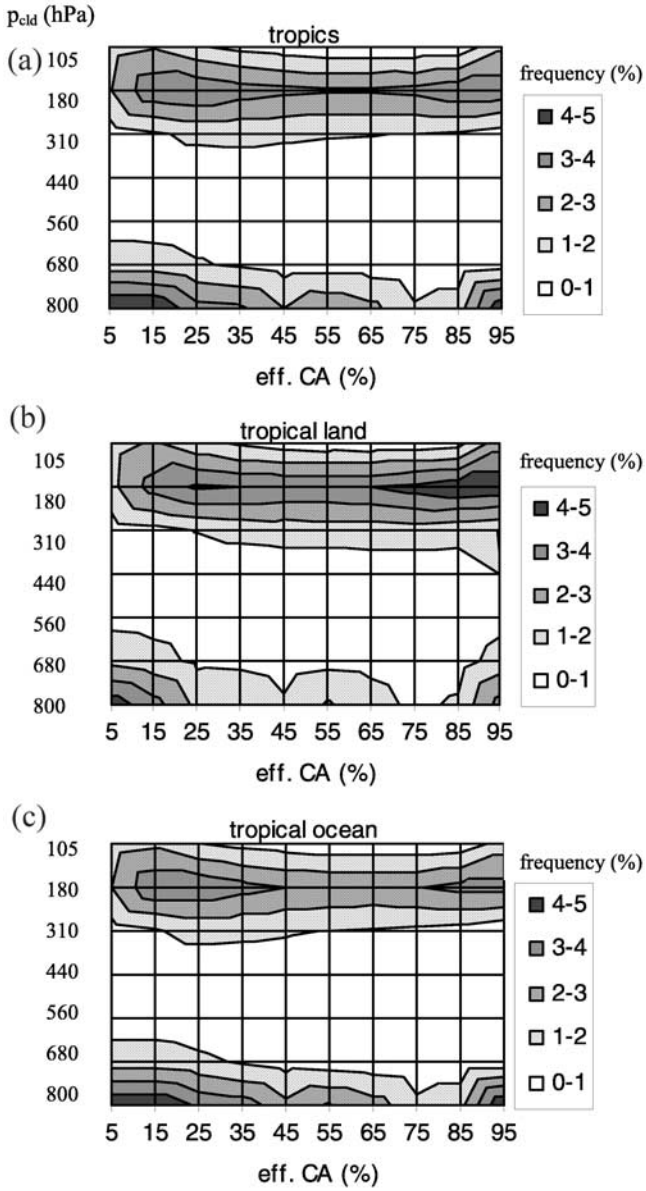

Figure 13. Two-dimensional frequency distribution of effective cloud amount and pressure of highest cloud layers (a) in the tropics, (b) over tropical land, and (c) over tropical ocean.

scattered radiation at 532 nm from quasi-simultaneous LITE observations. Two different averaging methods for the LITE inversion have been studied. An apparent middle of the cloud system has been determined using retrieved cloud top and apparent base within the cloud system from the averaged LITE backscatter profiles within a $1^\circ \times 1^\circ$ grid. However, one has to keep in mind that this level can be biased in the case of optically thick clouds: The base of a thick cloud should be overestimated, because the lidar cannot pass completely through the cloud. The LITE profiles have to be averaged because of the low signal-to-noise ratio. Comparison to averages of cloud height using retrievals of each LITE spot has shown that the apparent cloud midlevel retrieved from averaged LITE profiles is only slightly higher than the average from the retrievals of each LITE spot in the case of heterogeneous cloud scenes. For thick clouds it is about 1 km lower than the one determined from every LITE spot. Probably there are some spots within the $1^\circ \times 1^\circ$ regions which let the lidar more penetrate into the thick layer cloud system.

[44] The cloud height determined by TOVS corresponds in general well to the height of the middle of the cloud: It coincides within 1 km and 1.5 km of the cloud midlevel determined by LITE for 53% of TOVS Path-B low-level clouds and 49% of TOVS Path-B high-level clouds, respectively. 22.5% of TOVS Path-B low-level clouds are covered by an additional very thin high cloud layer not detectable by TOVS. Comparing in these cases the TOVS cloud height with the second LITE cloud layer increases the overall agreement for low-level clouds to about 64%. High-level clouds appear more often in multilayer systems (about 75%) and are also vertically more extended. These cloud fields seem to be more often heterogeneous which makes a comparison with the LITE path covering only a small fraction of the $1^\circ \times 1^\circ$ grids of the TOVS observations more difficult.

[45] The height of maximum backscatter of most single-layer low-level clouds and high-level clouds is several hundred meters above the apparent cloud midlevel, because these are mostly thicker clouds and therefore the lidar signal does not penetrate as deep into the cloud. Thin high-level clouds, with underlying low-level clouds, provide a backscatter signal nearer to the apparent cloud midlevel. In this

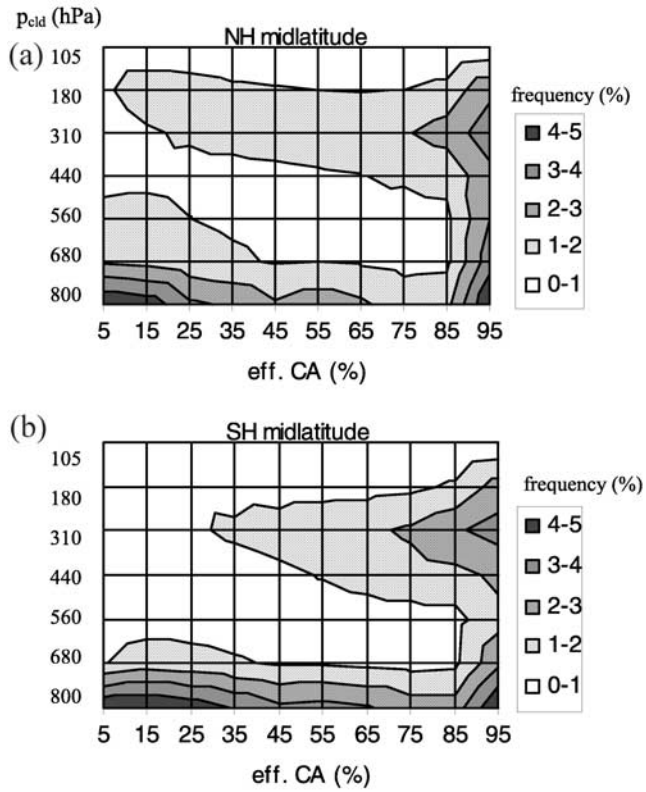

Figure 14. Two-dimensional frequency distribution of effective cloud amount and pressure of highest cloud layers in (a) NH midlatitudes and (b) SH midlatitudes.

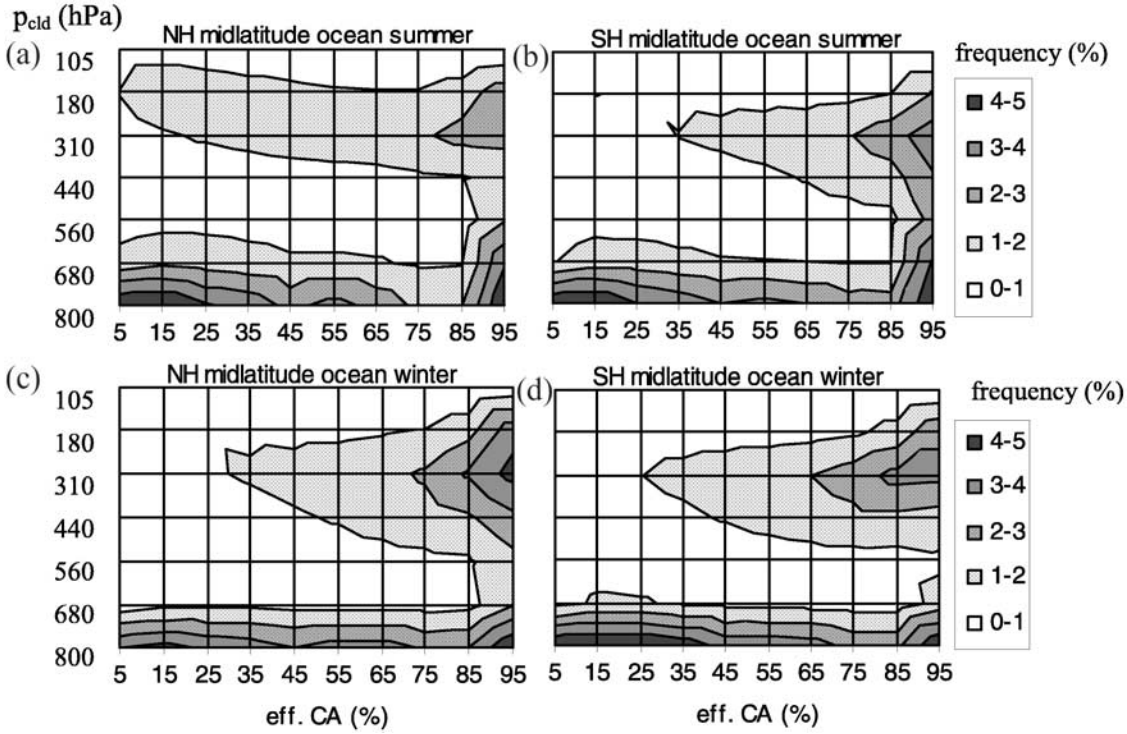

Figure 15. Two-dimensional frequency distribution of effective cloud amount and pressure of highest cloud layers over ocean in (a) NH midlatitudes during summer, (b) SH midlatitudes during summer, (c) NH midlatitudes during winter, and (d) SH midlatitudes during winter.

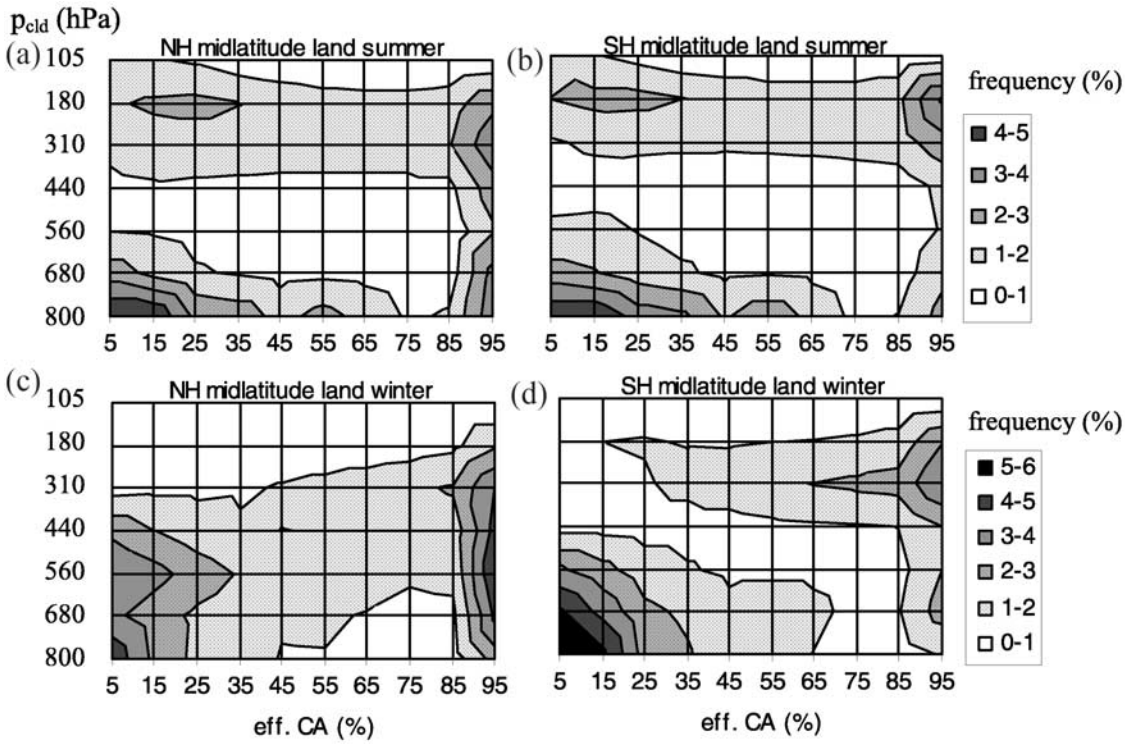

Figure 16. Two-dimensional frequency distribution of effective cloud amount and pressure of highest cloud layers over land in (a) NH midlatitudes during summer, (b) SH midlatitudes during summer, (c) NH midlatitudes during winter, and (d) SH midlatitudes during winter.

case, the retrieved TOVS Path-B cloud height is on average 280 m underestimated.

[46] Using 8 years of TOVS Path-B statistics on the highest cloud layers to study pressure distributions of the highest cloud layer weighted by effective cloud amount in different latitude bands has revealed that high clouds have the lowest pressure in the tropics, because of a higher tropopause, and in these regions there are nearly no cloud systems with the highest cloud layers in the middle troposphere. The Southern Hemisphere (SH) midlatitudes are mostly covered by low-level clouds. Seasonal differences in the Northern Hemisphere (NH) midlatitudes, with more equally distributed cloud altitudes in winter, are mostly caused by changes over land. In general, slightly lower cloud heights and slightly thicker clouds in the SH midlatitudes than in the NH midlatitudes can be explained by the small extent of land in the SH. The two-dimensional distributions of cloud pressure and effective cloud amount of the highest cloud layers could be quite useful for the evaluation of climate models.

[47] We have seen that the combination of active remote sensing instruments coupled with radiometers gives an important insight into the vertical structure of clouds and their resulting radiative properties. The Aquatrain missions which foresee a radar (CloudSat [*Stephens et al.*, 2002]) and a lidar (CALIPSO [*Winker et al.*, 2002]) flying in formation with the NASA Aqua satellite will give more interesting statistics.

[48] **Acknowledgments.** The TOVS Path-B data set has been processed at IDRIS. The authors want to thank the Analyze du Rayonnement Atmosphérique (ARA) group for their support as well as two anonymous reviewers for their thoughtful comments.

References

Baum, B. A., and B. A. Wielicki (1994), Cirrus cloud retrieval using infrared sounding data: Multilevel cloud errors, *J. Appl. Meteorol.*, *33*, 107–117.

Chevallier, F., F. Cheruy, N. A. Scott, and A. Chédin (1998), A neural network approach for a fast and accurate computation of longwave radiative budget, *J. Appl. Meteorol.*, *37*, 154–168.

Collis, R. T. H., and P. B. Russell (1976), Lidar measurements of particles and gases, in *Laser Monitoring of the Atmosphere*, *Topics Appl. Phys.*, vol. 14, edited by E. D. Hinkley, pp. 71–151, Springer, New York.

Jin, Y., W. B. Rossow, and D. P. Wylie (1996), Comparison of the climatologies of high-level clouds from HIRS and ISCCP, *J. Clim.*, *9*, 2850–2879.

Liao, X., W. B. Rossow, and D. Rind (1995), Comparison between SAGE II and ISCCP high-level clouds: 2. Locating cloud tops, *J. Geophys. Res.*, *100*, 1137–1147.

Mace, G. G., and S. Benson-Troth (2002), Cloud-layer overlap characteristics derived from long-term cloud radar data, *J. Clim.*, *15*, 2505–2515.

McCormick, M. P., et al. (1993), Scientific investigations planned for the Lidar In-space Technology Experiment (LITE), *Bull. Am. Meteorol. Soc.*, *74*, 205–214.

Menzel, W. P., and D. P. Wylie (2002), HIRS observations of a decline in high clouds since 1995, paper presented at 12th International TOVS Study Conference, Int. TOVS Working Group, Lorne, Victoria, Australia, 27 Feb. to 5 March.

Menzel, W. P., D. P. Wylie, and K. I. Strabala (1992), Seasonal and diurnal changes in cirrus clouds as seen in four years of observations with the VAS, *J. Appl. Meteorol.*, *31*, 370–385.

Platt, C. M. R., D. M. Winker, and M. A. Vaughan (1999), Backscatter to extinction ratio in cirrus observed in the layers of tropical mesoscale convective systems and isolated cirrus from LITE observations, *J. Appl. Meteorol.*, *38*, 1330–1345.

Rossow, W. B., and R. A. Schiffer (1999), Advances in understanding clouds from ISCCP, *Bull. Am. Meteorol. Soc.*, *80*, 2261–2287.

Scott, N. A., and A. Chédin (1981), A fast line by line method for atmospheric absorption computations: The Automized Atmospheric Absorption Atlas, *J. Appl. Meteorol.*, *20*, 802–812.

Scott, N. A., A. Chédin, R. Armante, J. Francis, C. J. Stubenrauch, J.-P. Chaboureau, F. Chevallier, C. Claud, and F. Chéruy (1999), Characteristics of the TOVS Pathfinder Path-B data set, *Bull. Am. Meteorol. Soc.*, *80*, 2679–2701.

Stephens, G. L., et al. (2002), The CLOUDSAT mission and the A-train, *Bull. Am. Meteorol. Soc.*, *83*, 1771–1790.

Stubenrauch, C. J., A. D. Del Genio, and W. B. Rossow (1997), Implementation of sub-grid cloud vertical structure inside a GCM and its effect on the radiation budget, *J. Clim.*, *10*, 273–287.

Stubenrauch, C. J., A. Chédin, R. Armante, and N. A. Scott (1999a), Clouds as seen by infrared sounders (3I) and imagers (ISCCP), part II: A new approach for cloud parameter determination in the 3I algorithms, *J. Clim.*, *12*, 2214–2223.

Stubenrauch, C. J., A. Chédin, R. Armante, and N. A. Scott (1999b), Clouds as seen by infrared sounders (3I) and imagers (ISCCP), part III: Combining 3I cloud parameters and ISCCP for better understanding of cloud radiative effects, *J. Clim.*, *12*, 3419–3442.

Stubenrauch, C. J., and the CIRAMOSA Team (2004), Final report on the European Environmental project EVK2-CT-2000-00063, 99 pp., Eur. Comm., Brussels. (Available at http://www.lmd.polytechnique.fr/CIRAMOSA/Welcome.html)

Wang, J., W. B. Rossow, T. Uttal, and M. Rozendaal (1999), Variability of cloud vertical structure during ASTEX from a combination of rawinsonde, radar, ceilometer and satellite data, *Mon. Weather Rev.*, *127*, 2484–2502.

Wang, J., W. B. Rossow, and Y. Zhang (2000), Cloud vertical structure and its variations from a 20-year global rawinsonde data set, *J. Clim.*, *13*, 3041–3056.

Winker, D. M., and C. R. Trepte (1998), Laminar cirrus observed near the tropical tropopause by LITE, *Geophys. Res. Lett.*, *25*, 3351–3354.

Winker, D. M., J. Pelon, and M. P. McCormick (2002), The CALIPSO mission: Spaceborne lidar for observation of aerosol and clouds, paper presented at Asia-Pacific Symposium on Remote Sensing of the Atmosphere, Environment and Space, Int. Soc. for Opt. Eng., Hangzhou, China, 23–27 Oct.

Wylie, D. P., and W. P. Menzel (1989), Two years of cloud cover statistics using VAS, *J. Clim.*, *2*, 380–392.

Wylie, D. P., and P.-H. Wang (1997), Comparison of cloud frequency data from the high-resolution infrared radiometer sounder and the Stratospheric Aerosol and Gas Experiment II, *J. Geophys. Res.*, *102*, 29,893–29,900.

Wylie, D., P. Piironen, W. Wolf, and E. Eloranta (1995), Understanding satellite cirrus cloud climatologies with calibrated lidar optical depths, *J. Atmos. Sci.*, *52*, 4327–4343.

Young, S. A. (1995), Analyses of lidar backscatter profiles in optically thin clouds, *Appl. Opt.*, *34*, 7019–7031.

Young, S. A. (2001), An investigation into the performance of algorithms used to retrieve cloud parameters from LITE lidar data, and implications for their use with PICASSO-CENA lidar data, *CSIRO Atmos. Res. Tech. Pap.*, *53*, 47 pp., Commonw. Sci. and Ind. Res. Org., Melbourne, Victoria, Australia.

F. Eddounia and C. J. Stubenrauch, Laboratoire de Météorologie Dynamique, IPSL, CNRS, Ecole Polytechnique, F-91128 Palaiseau cédex, France. (stubenrauch@lmd.polytechnique.fr)

L. Sauvage, Leosphere, Inc., 134 av. Parmentier, F-75011 Paris, France.